Bioinspired, Stimuli-Responsive, Multifunctional Superhydrophobic Surface with Directional Wetting, Adhesion, and Transport of Water

*Yang Liu, Xiaowen Wang, Bin Fei, Huawen Hu, Chuilin Lai, and John H. Xin**

A novel smart stimuli responsive surface can be fabricated by the subsequent self-assembly of the graphene monolayer and the TiO_2 nanofilm on various substrates, that is, fabrics, Si wafers, and polymer thin films. Multiscale application property can be achieved from the interfacial interaction between the hierarchical graphene/TiO_2 surface structure and the underlying substrate. The smart surface possesses superhydrophobic property as a result of its hierarchical micro- to nanoscale structural roughness. Upon manipulating the UV induced hydrophilic conversion of TiO_2 on graphene/TiO_2 surface, smart surface features, such as tunable adhesiveness, wettability, and directional water transport, can be easily obtained. The existence of graphene indeed enhances the electron–hole pair separation efficiency of the photoactive TiO_2, as the time required for the TiO_2 superhydrophilic conversion is largely reduced. Multifunctional characteristics, such as gas sensing, droplet manipulation, and self-cleaning, are achieved on the smart surface as a result of its robust superhydrophobicity, tunable wettability, and high photo-catalytic activity. It is also revealed that the superhydrophilic conversion of TiO_2 is possibly caused by the atomic rearrangement of TiO_2 under UV radiation, as a structural transformation from {101} to {001} is observed after the UV treatment.

1. Introduction

It is not surprised to discover that the great nature has furnished the livings with endless wonders of surface functions and structural design. It has been long since people began to realize the incomparable efficiency of such natural surfaces in self-cleaning, liquid transportation, antiicing, dry adhesion, drag reduction, antifouling, etc.[1] As a result, enormous research attempts have been devoted to mimic the composition as well as the structure of these surfaces in studies termed as biomimetics or bioinspiration. For example, artificial self-cleaning surface has been realized by mimicking the lotus leaf, in order to facilitate the unique function of the "lotus effect" on various substrates.[2] Moreover, upon mimicking the micro- to nanoscale structural roughness of the natural plants and insects, engineered superhydrophobic surfaces with tunable contact angle (CA) and hysteresis have also been fabricated by carbon nanotubes, polymers, and metal oxides, using the techniques such as chemical deposition, sol–gel, etching, or nanoprinting.[3] Directional surfaces with controllable liquid transportation properties, i.e., water condensation and collection, are also achieved on the poly(methyl methacrylate)-nylon fibers, patterned poly(acrylic acid)/poly(allylamine hydrochloride)/SiO_2/semi-fluorosilane superhydrophobic surface and conical copper wire by mimicking the special hydrophilic/hydrophobic region distribution of spider silk, Namib beetle's back, and cactus spines, respectively.[4] Furthermore, antiicing, dry adhesion, and drag reduction superhydrophobic surfaces are obtained by mimicking the Nepenthes pitcher plants, gecko appendage, and water strider legs.[5] The antifouling effect of the superhydrophobic turkey egg surface has also been discovered recently, which can serve as a cost-effective model for the development of artificial antibacteria surfaces.[6]

Compared to the natural biological surfaces, the functions of the artificial superhydrophobic surfaces are generally determined by their intrinsic compositions and structures, which make them relatively stationary to the external stimuli. However, natural surface and interface are generally stimuli-responsive. The examples include the self-healing of the living organism tissue surface and the snapping motion of the Venus flytrap originated from the elastic instability at the air–solid interface, or the switchable adhesion force of gecko toe pad and butterfly wings. The stimuli-responsive features of the natural surfaces make them extremely adaptable and durable to the surrounding environment, so that the overall bioecology performance can be promoted to the optimal level.[7] With emerging demands of functionality and adaptability, it is obvious that the structural design of static superhydrophobic surface (SHS) cannot provide a reasonable solution to overcome the functional and performance challenges. Bioinspired,

Y. Liu, X. Wang, Dr. B. Fei, H. Hu, Dr. C. Lai, Prof. J. H. Xin
Nanotechnology Centre
Institute of Textile and Clothing
The Hong Kong Polytechnic University
Hong Kong SAR, 999077 P. R. China
E-mail: john.xin@polyu.edu.hk

DOI: 10.1002/adfm.201501705

stimuli-responsive, directional engineered surfaces with order hydrophobic/hydrophilic region distribution are the state-of-the-art design criteria for constructing the high performance artificial surfaces.[8] Issues such as environmental adaptation, durability, efficiency, and renewability can also be addressed by integrating the design criteria during the construction of the multifunctional engineered surfaces.

Enormous functional combinations and possibilities can be generated on the surface with tunable wettability by integrating the criteria of biomimicry and stimuli-responsiveness. Utilizing the intrinsic surface chemistry and anisotropic wettability constructed on the bioinspired artificial surfaces, diverse functions such as self-cleaning, microfluid manipulation, directional nucleation and transport of water, can be triggered by the corresponding external stimuli.[9] Directional surface with unidirectional liquid transport property and tunable wettability anisotropy can also be constructed by the assembly of bioinspired micro- to nanoscale hierarchical roughness features and the incorporation of the structural components responding to the externals. For example, directional water transport induced by the "Ratchet" effect can be obtained from the periodic asymmetric structures with anisotropic wettability, i.e., spider silks and butterfly wings.[10] On the other hand, the stimuli-responsive surface facilitates the structural change, bond breaking, ionization, and functional group formation when exposing to proper stimuli such as electric field, pH, temperature, mechanical force, and light radiation. As a result, the molecular transformation would induce a chain effect on the polymeric network (polymer, hydrogel, TiO_2, etc.) of the stimuli-responsive surface and produces drastic changes on the surface wettability, tenacity, optoelectronic, electrical conductivity, and thermomechanic properties.[11] Smart material functions, including control drug release, biosensors, fog collection, cell culture, nanofiltration membrane and anticorrosive coatings, can then be readily obtained.[12] It is envisaged that multifunctional smart surfaces with both intrinsic programmable and external-specified functions can be designed and realized in the interdisciplinary of biomimicry and stimuli-responsiveness. In this case, optimal composite and hierarchy design can be applied and multiscale functions including self-cleaning, droplet adhesion, self-healing, antifouling, drag reduction, drug release and biosensing can be achieved respectively. To speak further, the smart multiscale functions can be manifested by maintaining the intrinsic functions of the structural components while enhanced functionalities are generated from the synergistic effect induced by the extensive interfacial interaction between the hierarchically structured components. With the urgent demand for the highly integrated and high performance engineered systems, this design criterion of multifunctional smart surface would be one of the most viable solutions among the existing tactics.

Herein we report a novel and facile fabrication method of a multifunctional smart surface which integrates the advantages of both biomimicry and stimuli-responsiveness. This smart surface was constructed by a two-layer self-assembly method on a fabric substrate. First, a graphene monolayer was assembled onto the fabric substrate (cotton, etc.) by a dipping-reducing method. Subsequently a TiO_2 nanofilm was deposited onto the graphene monolayer by the dip-pad-curing method. This nanoscale composite surface is much intriguing as unique electronic, optical, and thermal properties of graphene and TiO_2 are combined and a synergistic enhancement is also achieved. Moreover, the simple fabrication technique renders environmental-friendly and scalability, which are essential for the future industrial-scale production and application.

2. Results and Discussion

2.1. Surface Structural Characteristics of the Graphene-TiO_2 Coated Cotton Fabric

The cotton fabric was chosen as the sample substrate to demonstrate the smart surface characteristics. The surface features of this graphene-TiO_2 coated cotton fabric (GT fabric) are shown in **Figure 1**. The GT fabric shows a micro- to nanoscale surface roughness feature as the nanofilm with bright contrast can be observed on both of the fabric surface in macroscale and the individual fibers in microscale (Figure 1a–c). The nanofilm is visually smooth and extended through the longitudinal direction of fiber (Figure 1d). However, at higher magnification, this nanofilm shows a nanoscale roughness feature as densely packed TiO_2 nanoparticles (NPs) are composing the film surface (Figure 1e,f). This hierarchical nanofilm assembly shows features similar to the lotus leaf and butterfly wings;[13] as the underlying graphene coated microfibrous structure endows the fabric with moderate hydrophobicity and provides the microroughness while the film formed by densely packed nanoparticles renders enhanced nanoroughness feature and endows the surface with superhydrophobicity (CA = 151°).

The GT fabric exhibited a stable superhydrophobic property with the water CA of 151° (**Figure 2**i: inset). "Stable" here is referring to the water droplet remains its shape on the GT fabric surface without being absorbed by the underlying cotton fibers. In other words, the droplet on the GT fabric could remain in the Cassie state for the experimental duration, due to the biomimic hierarchically layered structures of graphene and TiO_2 NPs. In comparison, even though the TiO_2 NP coated cotton had a higher CA of 154° (Figure 2c: inset), a rapid Cassie to Wenzel transition was observed to occur within minutes, which had the droplet adsorbed by the fibers and in turn made the surface hydrophilic (Figure S9, Supporting Information). The unique self-assembling process of the graphene and TiO_2 NP layer on the fiber surface was investigated by scanning electron microscopy (SEM). In the first stage, the graphene oxide (GO) sheets wrapped on the fiber surface due to the hydrophobic interaction (Figure 2e,f). Characteristic fold and creases of graphene can be observed as well (Figure 2f: arrow pointed area). However, the fibers are still hydrophilic at this stage, similar to the bare cotton surface (Figure 2a,b). After being reduced to graphene, the original GO sheets still maintain a strong interfacial adhesion to the fiber substrate, as indicated by the compact surface coverage of the graphene coated fibers (Figure 2g,h). The as-obtained graphene surface is obviously rougher than the GO surface, which is possibly due to

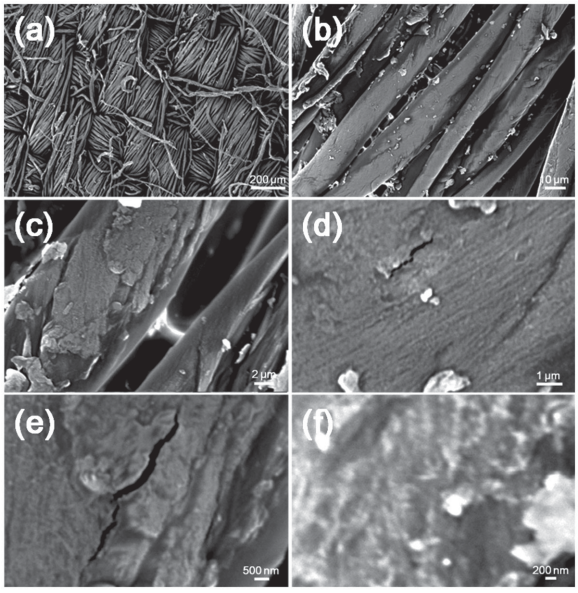

Figure 1. SEM images showing the micro- to nanoscale surface features of the GT fabrics. Scale bar (a–f): 200, 10, 2, and 1 µm, and 500 and 200 nm, respectively.

the structural deformation of the graphene basal plane during reduction.[14] The graphene surface is also hydrophobic with a contact angle of 138°, indicating the graphene single layer coating is insufficient to achieve superhydrophobicity. However, after the deposition of the TiO_2 NP nanofilm, stable superhydrophobicity can be achieved on the GT fabric as a result of the self-assembled hierarchical structured surface with dual roughness.

2.2. Stimuli-Responsive Wettability Control and Water Transport on the GT Fabric

Stimuli-responsiveness can be realized on the GT fabric surface utilizing the UV-induced superhydrophilicity of the TiO_2 NP film. Upon UV irradiation, the wettability of the TiO_2 nanofilm surface can be easily tuned from superhydrophobic to superhydrophilic, as a result of the surface structural change of the TiO_2 NPs during the UV process.[15] Thus patterning surface with controlled adhesion and directional water transport can be achieved on the GT fabric. Upon irradiation with a 365 nm UV lamp (0.457 mW cm^{-2}), the contact angle of the GT fabrics changed from superhydrophobic (151°) to superhydrophilic (0°) within a short period of 3 h (**Figure 3**a). Therefore by tuning the UV duration, different wetting characteristic from superhydrophilic to superhydrophobic can be facilely obtained on the GT fabric surface. Moreover, the surface adhesion of the fabric also exhibited significant enhancement after the UV radiation. The change of water droplet adhesion from sliding to sticky was readily observed after UV the fabric for 30 min. With increasing droplet volume from 10 to 50 µL, the sliding angle of the GT fabric changed from 75° to 32°, indicating a depinning effect induced by gravity (Figure 3b). However, after 30 min UV irradiation to the fabric surface, it became adhesive for the droplet with a volume below 30 µL; while in the higher volume region (35–50 µL) the gravity effect dominated and the difference between the UV (red) and non-UV (blue) fabric was negligible. This UV-induced droplet adhesion is important for the applications such as microfluidic storage, transport, or surface patterning on the GT fabric. Interestingly, due to the wettability anisotropy at the two sides of the GT fabric, a transportation process was observed between the two fabric sides driven by the surface energy gradient.[16] In fact, due to the thickness of the fabric, the fabric side facing the UV light received the maximum UV intensity while the opposite side received the minimum. Therefore, a surface energy gradient was generated between the two fabric sides which can drive the droplet on the back side (UV opposing) directionally to the face side (UV facing). The water droplets exhibited different behaviors on the two fabric sides after UV the GT fabric for 3 h and convert the UV-facing side of the fabric to superhydrophilic. The droplets spread almost instantly on the face side and retained their spherical shapes on the back side while being gradually transported across the fabric thickness to the face side (Figures S10 and S11, Supporting Information). There was an obvious time gap between the droplet absorption process on the fabric face side and the transport process on the back side. In general, the time required for absorption is much shorter than transport, evidencing the existence of the energy gradient across the fabric axial direction. Obviously the UV-facing side has the highest surface energy while the back

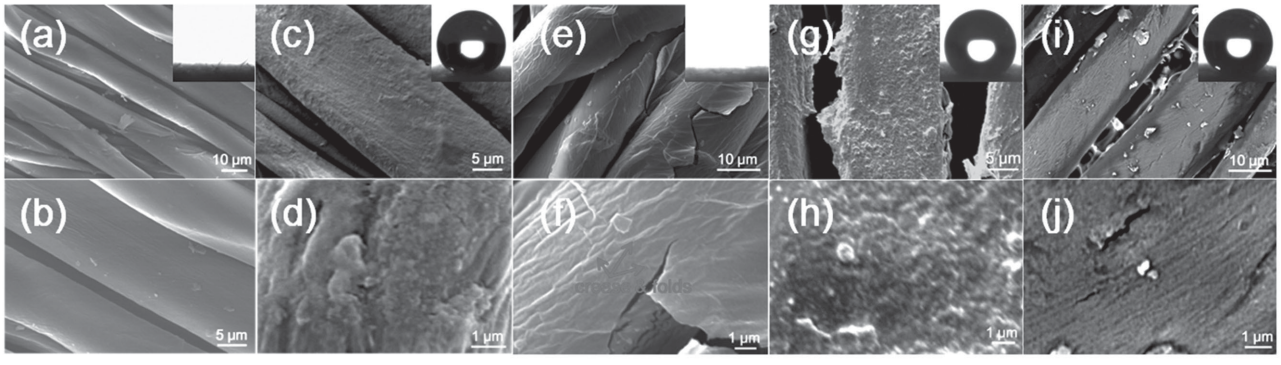

Figure 2. SEM and magnified SEM images showing the surface morphologies of bare cotton a,b), TiO_2 NP coated c,d), GO coated e,f), graphene coated cotton fabric g,h), and the GT fabric i,j). Insets show the shape of a 2 µL water droplet on the corresponding surfaces, respectively.

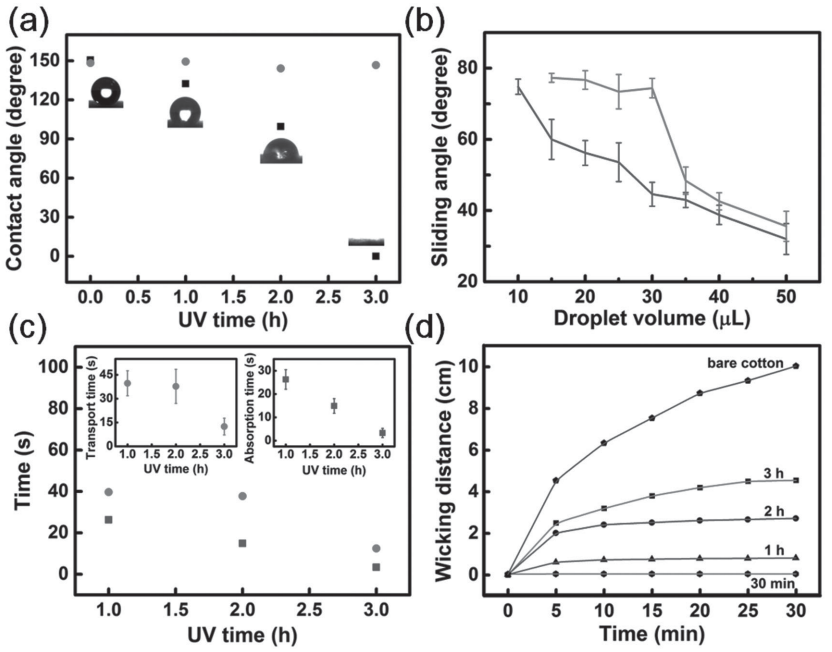

Figure 3. a) Contact angle versus UV time for the GT fabric face side (squares) and back side (circles) to the UV light. b) Sliding angle versus droplet volume for the GT fabric before (bottom) and after (top) 30 min UV irradiation. c) Droplet (2 μL) absorption (squares) and transport (circles) speed (in seconds) on the GT fabrics with different UV irradiation time (1, 2, and 3 h). Insets show the transportation (left) and adsorption (right) speed with Y errors. Each data point is the average of five parallel measurements. d) Wicking test results for the GT fabric irradiated with UV light for 30 min and 1, 2, and 3 h, respectively.

side attains the lowest (Figure 3c). With the increase of UV-radiation time, a decrease in both the absorption and transport time can be observed, indicating the enhanced hydrophilicity of the fabric. The directional water transport property was also durable, which could be maintained more than one month. Even if the fabric surface was turned into superhydrophilic after 3 h UV radiation, the water transport within its capillary network was still impeded in the radial direction, as indicated by the wicking test (Figure 3d). However, this phenomenon is possibly due to the limited penetration distance of the UV light with respect to the thickness of the fabric. This directional water transport behavior of the fabric is of particular importance for applications such as biofluid collection, antisweating, and moisture management, as a rapid water transport is required at the solid–liquid–air interface.

2.3. Mechanism Study of the UV Superhydrophilic Conversion

The smart stimuli-responsiveness of the GT surface is largely dependent on the photo-induced superhydrophilic properties of the TiO_2 NPs. Even though the superhydrophilic conversion of the TiO_2 thin films has been observed in 1997, the underlying mechanism is still unclear.[17] Extensive research effort has been devoted to uncover the phenomenon and three major theories have been proposed: (i) the photo-generated holes reacted on the TiO_2 surface, forming new surface hydroxyl groups and oxygen vacancies, which lowered the surface tension significantly;[18] (ii) the adsorbed organics on the TiO_2 surface were decomposed during UV due to the self-cleaning effect of the TiO_2, resulting in a purified surface composition with higher surface energy;[19] (iii) the heating effect of UV increased the temperature of the TiO_2 surface and reduced the adsorbed water molecules, which in turn lowered the surface tension of the water clusters.[20] By investigating the UV-induced superhydrophilicity on the GT fabric, we have also discovered an interesting phenomenon which may possibly shed light on the true nature of the TiO_2 superhydrophilic conversion.

A GT surface was constructed on the silicon wafer by the subsequent deposition of a self-assemble graphene monolayer and TiO_2 NP nanofilm, which is similar to the GT fabric-making process. This GT surface was subjected to 3 h UV irradiation and its surface characteristics were measured by atomic force microscopy (AFM). Before the UV treatment, the GT surface was majorly composed of TiO_2 NPs with sizes ranged from 12 to 39 nm (**Figure 4**a). Roughness was also provided by the densely packed TiO_2 NPs which also formed a thin film on top of the graphene layer. However, after 3 h UV irradiation, a clear surface morphology change was observed. The mean particle size, as well as the roughness, increased markedly for the GT surface (Figure 4b). The mean particle size was increased from 24 to 31 nm; and the R_a, R_q, R_{max} of the UV irradiated sample also showed notable increment, i.e., the R_q was increased from 4.65 to 5.34 nm (Table S1, Supporting Information). The surface boundaries were also been expanded and fused after UV irradiation, as indicated by the phase images (Figure 4c,d). This structural change can be seen more clearly in the 3D structure of the GT surface (Figure 4e,f), as the sharp peaks on the surface were merged with each other, resulting in a clear surface ripening and volume expansion. The surface volume expansion of the semiconductor NP after UV irradiation was examined extensively and was linked to the phase transformation induced by the photon energy of the UV light.[21] However, this microstructural change indeed accompanies with the atomic rearrangements of the TiO_2 NPs, which could be the key factor for the superhydrophilic conversion of the TiO_2 thin film.

In order to investigate the effect of UV on the atomic structure of TiO_2, a TiO_2 NP nanofilm was casted on a copper grid and transmission electron microscopy (TEM) was used for the characterization. Before the UV treatment, the TiO_2 NP nanofilm was mainly composed of NPs around 10–30 nm, which coincided with the AFM results (**Figure 5**a). The as-obtained NPs were single crystals with a fringe spacing of 0.35 nm, corresponding to the (101) lattice reflection of anatase TiO_2 (Figure 5b). It thus revealed that the TiO_2 nanofilm was composed of NPs with the {101} facet exposed on the surface, which was more thermodynamic stable compared to the other

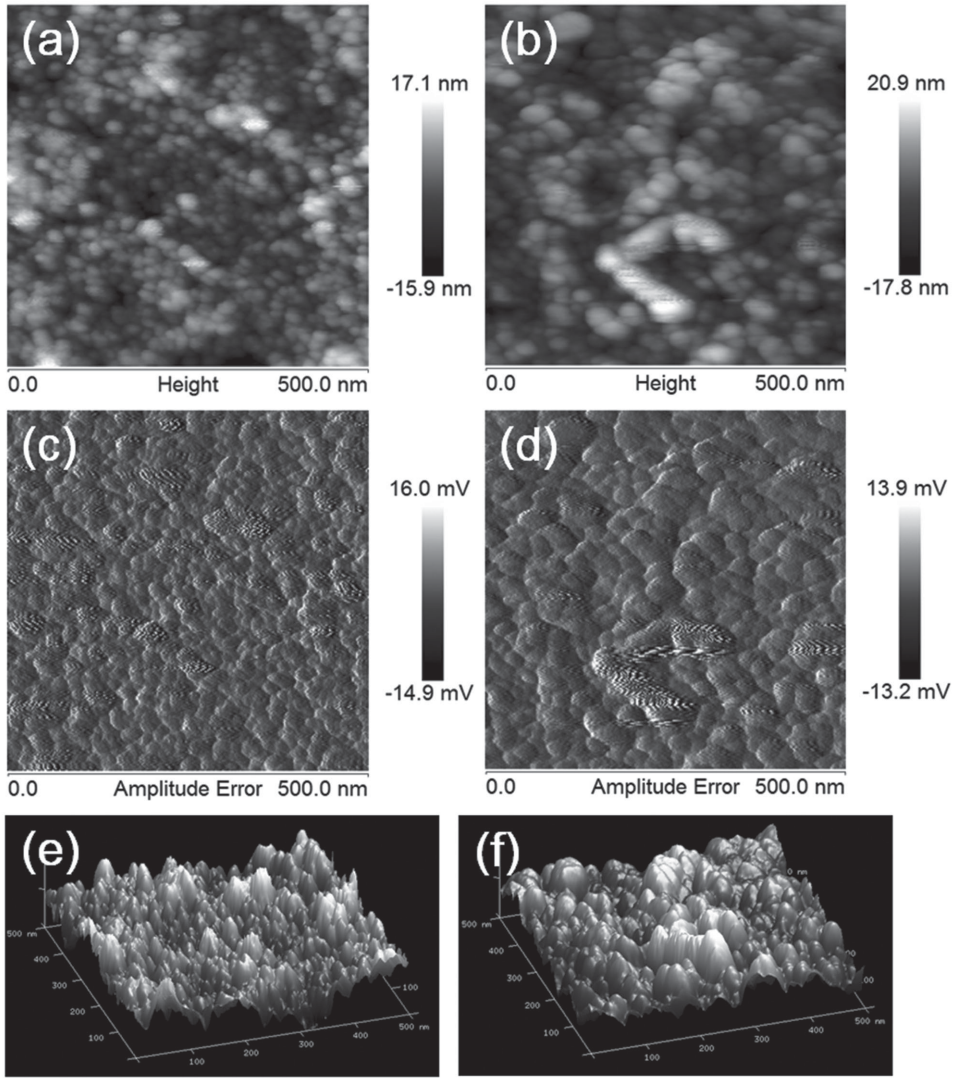

Figure 4. AFM, amplitude error, and corresponding 3D surface structure images of the GT surface before a,c,e) and after b,d,f) 3 h UV irradiation.

anatase facets.[22] The single-crystal TiO_2 NPs were generally oriented along the [001] direction, as indicated by the interfacial angle of 68.3° between {101} and {001} (Figure 5b(1)); as well as the enhanced (004) intensity of the X-ray diffraction (XRD) spectrum (Figure S7, Supporting Information). Interestingly, after 3 h UV irradiation of the nanofilm, a structural transformation at the atomic scale can be observed. The TiO_2 NPs started to merge and fuse with each other to form larger particles and particulate clusters (**Figure 6**a). This macroscale change was considered originated from the microscale reconstruction of the TiO_2 atomic structure. The merging and fusing of the NPs can be observed more clearly in the high-resolution TEM (HRTEM) image (Figure 6b). But the more significant phenomenon is the conversion of the exposed facet of the TiO_2 NPs from {101} to {001}, corresponding to the change of the fringe spacing from 0.35 to 0.23 nm (Figure 6b(1–12)). Compared to the {101} facet, the {001} facet has a higher surface energy which contains active unsaturated Ti atoms and active oxygen atoms.[23] In other words, the {001} facet is more chemically active than the {101} facet, and the conversion of the {101} to {001} of the anatase TiO_2 is considered to be the true nature of the superhydrophilic conversion.

The structural transformation of the nanocrystalline during UV irradiation has been extensively studied.[24] Generally speaking, two major phenomena are associated with the structural transformation of the nanocrystals, one is the rearrangement of the crystal facets and the other is the volume change of the crystalline structure.[25] In the specific case of the TiO_2 nanofilm, a surface heterojunction can be formed between the {101} and {001} facets due to the Fermi level alignment at the contact interface of these two facets.[26] This surface heterojunction can facilitate the electron–hole pair separation and serve as the pathway for the photo-generated electrons and holes to transfer to the {101} and {001} facets, respectively.[27] Hence, as the TiO_2 nanofilm is irradiated by the 365 nm (≈3.4 eV) UV lamp, which has a higher photon energy than the band gap of

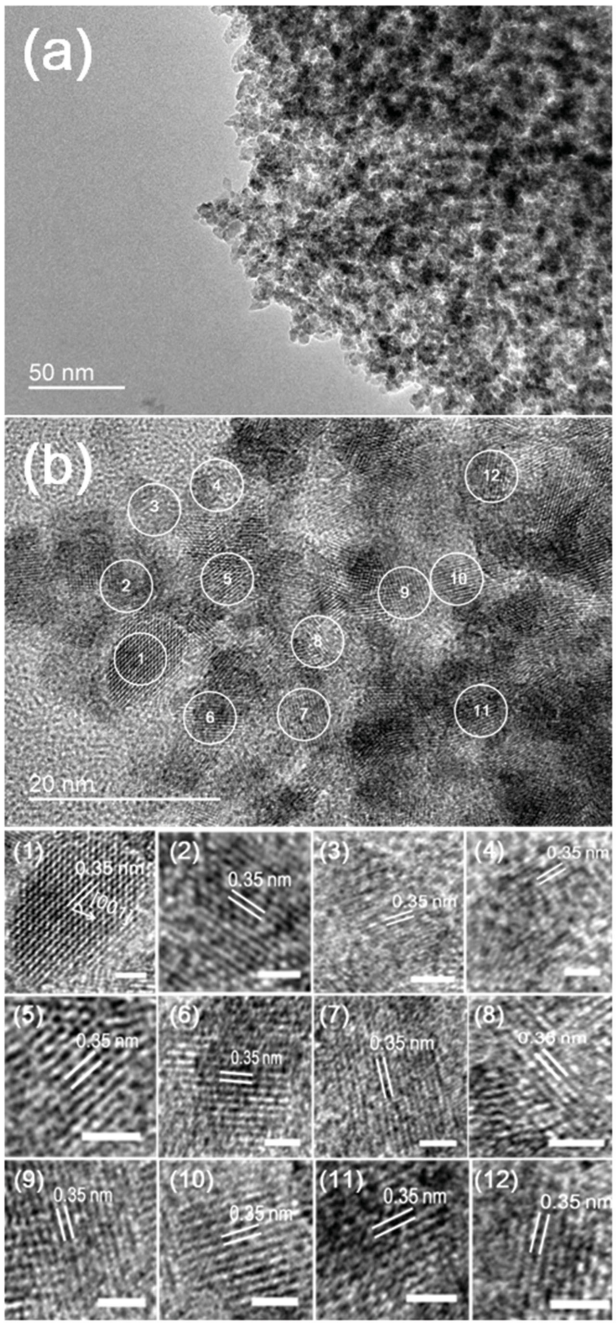

Figure 5. a) TEM and b) HRTEM images of the TiO_2 nanofilm. The TiO_2 NPs are numbered and the corresponding HR images are shown. Scale bar: 2 nm.

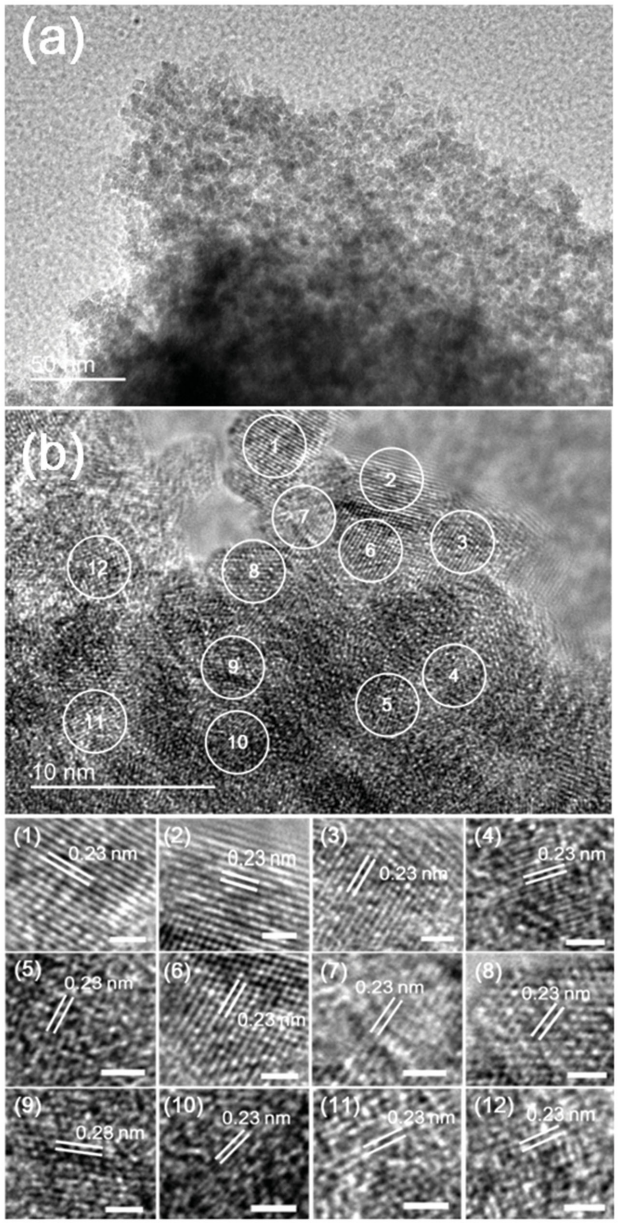

Figure 6. a) TEM and b) HRTEM images of the TiO_2 nanofilm after 3 h UV irradiation. The TiO_2 NPs are numbered and the corresponding HR images are shown. Scale bar: 1 nm.

the anatase TiO_2 (≈3.2 eV), the electron–hole pair can be generated on the nanofilm surface. At the primary stage, as the {101} facet dominates, the recombination of photo-generated electrons and holes happened extensively at the surface facet, resulting in the large amount of heat release.[28] The released heat accumulates on the crystal surface and eventually induces a partial melting of the crystals, which in turn brings forth the rearrangement of the atomic lattice of the TiO_2 crystals, possibly under a solid–liquid pathway, and leads to the surface facet conversion from {101} to {001}. The conversion from {101} to {001} facet on the TiO_2 NP surface is considered the key factor which induces the superhydrophilic conversion. As a consequence, while more {001} facet is produced from this process, enhanced electron–hole pair separation efficiency can be achieved on the TiO_2 NPs, as the electrons are drawn to the {101} facet and the holes are moved to the {001} facet. The holes on the {001} facet thus will continue to react with the TiO_2 itself, breaking the bonds between the Ti and O, and create new surface hydroxyl groups by reacting with the coordinated water molecules. The greatly enhanced hydroxyl group density on the exposed {001} facet thus would result in the

superhydrophilicity on the TiO_2 surface, despite the initial hydroxyl group density on the {001} facet (7.0 nm^{-2}) is much higher than the {101} facet (5.1 nm^{-2}).[29] On the other hand, the photo-generated holes can also react with the surface organics, resulted in the decomposition of these surface contaminants and a surface energy increase; which also lowers the surface contact angle noticeably.[30] The photo-generated holes are indeed indispensable for the superhydrophilic conversion. However, the key step for the holes to participate in the surface reaction may rest on the structural transformation of the exposed TiO_2 facets from {101} to {001}, otherwise the holes may be consumed in the photo-recombination process.

It was also observed that the existence of the graphene monolayer can drastically enhance the superhydrophilic conversion rate on the TiO_2 nanofilm surface. XPS analysis indicated that the GT surface generally possessed a higher surface binding energy than the TiO_2 thin film surface. In terms of the O1s spectra, the differences were 0.2 eV before and after the UV radiation (Figure S13a, Supporting Information). And for the Ti2p spectra, the differences were 0.1 eV before and after UV (Figure S13b, Supporting Information). The higher surface binding energy for the GT surface in both the pristine and UV states thus manifested a lower surface energy state of the GT surface, as compared to the TiO_2 thin film surface.[31] More surface hydroxyl groups can also be generated on the GT surface upon UV radiation (Figure S14a,b, Supporting Information) compared to the TiO_2 thin film surface (Figure S14c,d, Supporting Information), indicating a different superhydrophilic conversion pathway on these two surfaces. However, in case of the GT surface, the lowering of TiO_2 surface energy with the existence of the graphene monolayer may attribute to the interfacial charge transfer interaction between the TiO_2 nanofilm and graphene monolayer.[32] This interfacial charge transfer interaction not only lowered the surface energy of the GT surface, resulting in a higher water contact angle (WCA), but also accelerated the superhydrophilic conversion of the TiO_2 surface noticeably. To examine the degree and extent of the interfacial charge transfer interaction, the UV radiation tests were performed on the GT surface, TiO_2 thin film and graphene thin film, respectively. It was observed that the WCA of the GT surface changed from 40.9° to 8.3° after 3 h UV irradiation (Figure S15a,d, Supporting Information), while the WCA of the TiO_2 thin film changed from 34.4° to 16.02° (Figure S15b,e, Supporting Information). Based on the WCA change versus UV time, a superhydrophilic conversion rate of 10.9° h^{-1} can be achieved on the GT surface, which was 79% faster than the rate on the TiO_2 thin film (6.1° h^{-1}). Interestingly, the WCA of the graphene thin film drastically increased from 52.7° to 79.9° (Figure S15c,f, Supporting Information), which can be possibly ascribed to the enhanced surface roughness induced by the UV radiation.

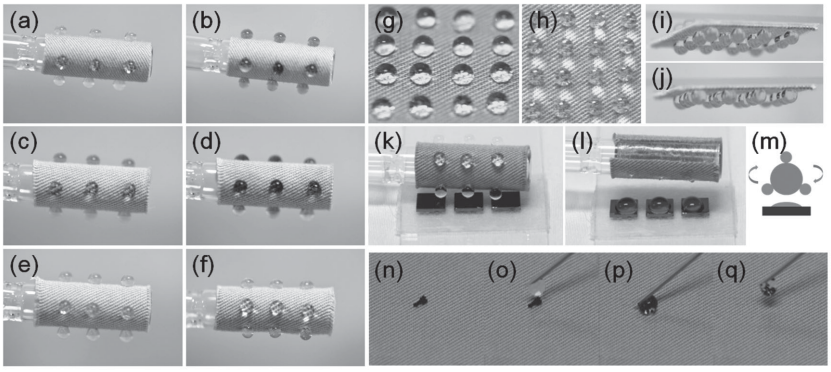

Figure 7. a–f) Flexible GT fabric-based droplet sensor arrays mounted on a glass rod. The droplet sensors are loaded with different indicators (a,b: Cu^{2+}; c,d: Congo red; e,f: Pd^{2+}) for the sensory of different stimuli (a,b: NH_3; c,d: HCl; e,f: ethylene diamine). g–j) A 4 × 4 array of droplets stored on the GT fabric surface, which remained stable at the 90° h) and 180° tilt i,j) configurations. k–m) The transport of droplet arrays on the GT fabric to a silicon wafer array. The droplets are transferred and mixed on the silicon wafers. n–q) Removal of the carbon nanotube powder from the GT fabric surface by a single droplet.

2.4. Applications of the GT Fabric in Microdroplet Devices and Water/Oil Separation

The smart stimuli-responsive GT fabrics can have wide-range applications in droplet manipulation and microfluidic devices. The TiO_2 nanofilm on the fabric enables the possible switchable wetting control and patterning on the fabric surface, which in turn realizes the fine manipulative actions of the droplets, i.e., storage, transfer, collection, and sensing.[33] More specifically, this low-cost, scalable GT fabric can serve as the ideal lab-on-a-chip device for the processing of the expensive biofluids and microdroplets. Practical application functions, such as self-cleaning, UV proofing, and antibacteria, can also be easily obtained on the GT fabric which makes it a quite promising candidate for the next-generation smart textiles.

Novel droplet sensors can be fabricated using the GT fabric through the casting of droplet arrays on the fabric surface. Due to the flexibility of the fabric, the droplet sensor can be mounted on various substrates with different geometrical features, i.e., glass sticks, metal meshes, or polymer thin films, indicating its wide-range adaptability in real-field applications. Furthermore, the droplet array can be loaded with different indicators for accurate sensing or multiple sensing purposes. Examples are given by the droplet arrays loaded with the metal ions, i.e., Cu^{2+} and Pd^{2+}, to sense the NH_3 (**Figure 7**a,b) and ethylene diamine (Figure 7e,f) gases. Selectivity can also be achieved by the incorporation of different-type indicators, i.e., Congo red, for the sensing of HCl gas (Figure 7c,d). Both qualitative and quantitative sensing can be achieved on the GT fabric-based droplet sensor. Rapid, high throughput sensory performance can also be readily achieved by the droplet permutation and indicator combination. In case of sensing the NH_3 gas, sensitivity as low as 6 ppm can be achieved on the fabric droplet sensor and the response time was typically within 30 s. Deepening of the blue color in the droplets was observed with increasing NH_3 gas concentration, indicating good sensing linearity of the droplet sensor (Figure S18, Supporting Information). On the other hand, droplet manipulations, including

storage, transfer and mixing are realized on the GT fabric surface as a result of the robust superhydrophobicity and water droplet adhesion provided by the GT fabric. A 4 × 4 droplet array was casted on the GT fabric surface and the individual droplet size was set to be 10 µL (Figure 7g). The droplets were remained stable on the fabric surface even at a tilt angle of 90° (Figure 7h) and 180° (Figure 7i,j), indicating the sufficient droplet adhesion provided by the GT fabric surface. It was speculated that the droplets were in the impregnating Cassie state after being casted onto the GT fabric surface, which assembled the "rose petal effect," as both high CA and high adhesiveness were observed.[34] The droplet arrays on the fabric surface can also be properly arranged and transferred to the other substrates. A GT fabric was mounted on the glass rod and a 3 × 3 droplet array was deposited on its curved surface (Figure 7k). Upon rotating the glass rod accordingly, the droplets on the fabric can be transferred to the silicon wafer underneath in a continuous and control manner (Figure 7l,m). In this regards, the transfer and mixing of the droplets were completed simultaneously in a single rotation cycle. This feature is useful in the microreactor applications as miniaturized chemical reactions can be carried out by the transfer and mixing of the microdroplets loaded with different reagents. It also reveals that simple microfluidic and lab-on-a-chip devices can be realized based on the GT fabric. Self-cleaning is another practical function for the GT fabrics, as the durability and reusability of the fabric can both be enhanced. Due to the robust superhydrophobic property of the GT surface, self-cleaning can be easily realized. For example, the carbon nanotube spread onto the fabric surface can be removed facilely by a single water droplet, without the observation of any powder or water residues (Figure 7n,q).

The superhydrophobic characteristic and porosity of the GT fabric make it an ideal filtration membrane for the water/oil separation application, which shows solid potential as the bargain solution for today's urgent environmental issue such as oil spills. A proof-of-concept filtration device was then assembled and the GT fabric was fixed at the filter head to serve as the filtration membrane for the water/oil mixture (**Figure 8**a). A mixture of water and chloroform (Figure 8b) was then poured into the glass tube. Subsequently, the portion of chloroform quickly permeated through the fabric and rested at the bottom of the flask (Figure 8c). On the contrary, the water phase was blocked by the fabric and remained in the glass tube, as a result of the superhydrophobicity of the GT fabric. No blue color residue can be observed in the glass tube, indicating the high separation efficiency of the GT fabric filtration membrane. By measuring the weight of chloroform before (W_0) and after (W_i) the separation process, the separation efficiency (R) was calculated to be 99.2% [$R = (W_i/W_0) \times 100\%$]. A flux as high as 3162 ± 128 L m^{-2} h^{-1} was obtained for the GT fabric filtration membrane during the separation of the water/chloroform mixture (The flux was calculated by measuring the flow volume permeated through the filtration area of the membrane in unit time and kept the input water/oil mixture height at 8 cm). This flux value is much higher than the conventional membranes used for water/oil separation (<500 L m^{-2} h^{-1}).[35] Therefore both high separation speed and efficiency can be obtained by the GT fabric, indicating its remarkable practical functions in water/oil separation. The pore structure of the GT fabric was also investigated (Figure S20, Supporting Information). It was found that the fabric was majorly composed of the inter-yarn pores and inter-fiber pores, with sizes of 21–56 and 0.2–6 µm, respectively. The pore size distribution of the GT fabric was close to the untreated woven cotton fabric, indicating the existence of GT surface did not markedly affect the underlying fabric structure.[36] It was also noteworthy that only a piece of the GT fabric was used during the separation, while multiple layers of the fabric can be used for the heavier separation tasks. In addition, different types of oil, i.e., hexane, dodecane, hexadecane, can also be separated by the GT fabric membrane effectively, revealing the wide-range applicability of the fabric to different water/oil mixtures (Figure S21, Supporting Information). However, when using the bare cotton fabric as the filter membrane, no separation occurred as a result of the hydrophilicity of bare cotton (Figure 8d).

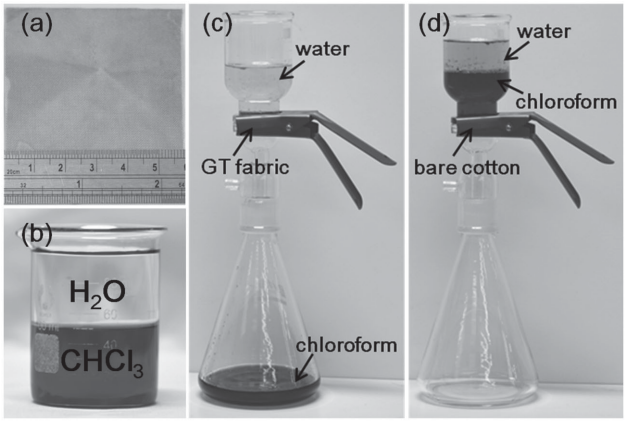

Figure 8. a) A 6 × 6 cm GT fabric used for the water/oil separation process. b) Mixture of water and chloroform showed clear phase separation, the chloroform was dyed with oil blue for clearer observation. c) The GT fabric was used as the filter membrane and the water/chloroform mixture was separated successfully. The chloroform penetrated through the fabric and rested at the bottom while water remained in the glass container. d) The bare cotton fabric was fixed as the filter membrane and the water/chloroform mixture was poured into the filter, no liquid passed through due to the hydrophilic nature of the cotton fabric.

3. Conclusions

In conclusion, using a two-layer self-assembly method, a smart stimuli-responsive superhydrophobic surface based on the hierarchical structure of graphene and TiO_2 nanofilm with bioinspired dual roughness, was constructed and applied onto the cotton fabrics. The surface exhibits tunable wetting, adhesion, and directional water transport properties, which provides a general protocol for applications such as moisture management, microfluidic control, self-cleaning, and water/oil separation. The unique smart surface properties and wettability control can be facilitated through manipulating the UV superhydrophilic conversion on the TiO_2 nanofilm, which is significantly accelerated by the graphene monolayer through the interfacial charge transfer interaction. It was also discovered that the superhydrophilic conversion on the TiO_2

nanofilm was induced by the microscopic atomic rearrangement on the TiO_2 lattice accompanied with the macroscopic film structural change such as volume expansion. The design of the novel smart stimuli-responsive surface incorporates the concept of environmental adaptability, multiscale tunable functions, and directionality. Providing the vast functional possibilities generated by the material combinations, i.e., graphene and TiO_2 in this case, this design criterion may help find out the optimal solution for the pressing demand for material adaptability and functions, where high performance, scalability, and cost effectiveness are the subjects of concern.

4. Experimental Section

Fabrication of the Graphene/TiO_2 Coated Cotton Fabric (GT Fabric): A 3 mg mL^{-1} GO dispersion was prepared by adding 90 mg of the as-prepared GO into 30 mL D.I. water. The dispersion was sonicated for 30 min to achieve homogeneous. A precut cotton fabric with known dimensions was then dipped into the GO dispersion for 30 s and transferred to a 50 mL aqueous solution containing 0.2 mL hydrazine monohydrate. The solution was then stirred for 5 min in order to achieve homogeneous and heated to 80 °C. The reduction of GO to graphene would take place during this stage and the solution was kept at 80 °C for 1 h. Eventually the GO adsorbed onto the fabric was reduced to graphene, as indicated by the black coating formed on the fabric surface. The as-obtained graphene structure was also confirmed by the TEM characterization (Figure S1, Supporting Information). The graphene coated fabric was then washed with copious D.I. water and dried at 60 °C. Afterwards, the TiO_2 nanofilm was applied onto the fabric through a dip-pad-dry-curing process. The fabric was first immersed in the TiO_2 sol–gel solution (1 wt%) for 5 min and then removed and padded through a vertical padder at the pressure of 2 kg cm^{-2} and speed of 5 rpm. The fabric was then dried in an 80 °C oven for 10 min and then cured at 160 °C for 3 min. Relatively homogeneous TiO_2 nanofilm was formed on the fabric surface after the curing process as indicated by the energy dispersive X-ray (EDX) mapping (Figure S4, Supporting Information). The schematic illustration of the GT fabric fabrication process was also shown in Scheme S1 (Supporting Information).

Supporting Information

Supporting Information is available from the Wiley Online Library or from the author.

Acknowledgements

The financial support from The Hong Kong Polytechnic University is gratefully acknowledged.

Received: April 27, 2015
Revised: June 4, 2015
Published online: July 14, 2015

[1] a) L. Feng, S. Li, Y. Li, H. Li, L. Zhang, J. Zhai, Y. Song, B. Liu, L. Jiang, D. Zhu, *Adv. Mater.* **2002**, *14*, 1857; b) M. J. Hancock, K. Sekeroglu, M. C. Demirel, *Adv. Funct. Mater.* **2012**, *22*, 2223; c) J. Lv, Y. Song, L. Jiang, J. Wang, *ACS Nano* **2014**, *8*, 3152.

[2] R. Furstner, W. Barthlott, C. Neinhuis, P. Walzel, *Langmuir* **2005**, *21*, 956.

[3] a) Y. Lai, F. Pan, C. Xu, H. Fuchs, L. Chi, *Adv. Mater.* **2013**, *25*, 1682; b) K. K. Lau, J. Bico, K. B. Teo, M. Chhowalla, G. A. Amaratunga, W. I. Milne, G. H. Mckinley, K. K. Gleason, *Nano Lett.* **2003**, *3*, 1701; c) Y. Lee, S. H. Park, K. B. Kim, J. K. Lee, *Adv. Mater.* **2007**, *19*, 2330; d) X. Zhang, F. Shi, J. Niu, Y. Jiang, Z. Wang, *J. Mater. Chem.* **2008**, *18*, 621; e) H. Y. Erbil, A. L. Demirel, Y. Avci, O. Mert, *Science* **2003**, *299*, 1377.

[4] a) Y. Zheng, H. Bai, Z. Huang, X. Tian, F. Q. Nie, Y. Zhao, J. Zhai, L. Jiang, *Nature* **2010**, *463*, 640; b) L. Zhai, M. C. Berg, F. C. Cebeci, Y. Kim, J. M. Milwid, M. F. Rubner, R. E. Cohen, *Nano Lett.* **2006**, *6*, 1213; c) J. Ju, K. Xiao, X. Yao, H. Bai, L. Jiang, *Adv. Mater.* **2013**, *25*, 5937.

[5] a) T. S. Wang, S. H. Kang, S. K. Tang, E. J. Smythe, B. D. Hatton, A. Grinthal, J. Aizenberg, *Nature* **2011**, *477*, 443; b) N. S. Pesika, H. Zeng, K. Kristiansen, B. Zhao, Y. Tian, K. Autumn, J. Israelachvili, *J. Phys.: Condens. Matter* **2009**, *21*, 464132; c) L. Jiang, X. Yao, H. Li, Y. Fu, L. Chen, Q. Meng, W. Hu, L. Jiang, *Adv. Mater.* **2010**, *22*, 376.

[6] L. D'Alba, D. N. Jones, H. T. Badawy, C. M. Eliason, M. D. Shawkey, *J. Exp. Biol.* **2014**, *217*, 1116.

[7] a) H. Kuroki, I. Tokarev, D. Nykypanchuk, E. Zhulina, S. Minko, *Adv. Funct. Mater.* **2013**, *23*, 4593; b) D. P. Holmes, A. J. Crosby, *Adv. Mater.* **2007**, *19*, 3589; c) F. Xia, L. Jiang, *Adv. Mater.* **2008**, *20*, 2842.

[8] K. Liu, X. Yao, L. Jiang, *Chem. Soc. Rev.* **2010**, *39*, 3240.

[9] a) G. D. Bixler, B. Bhushan, *Nanoscale* **2013**, *5*, 7685; b) J. M. Toonder, P. R. Onck, *Trends Biotechnol.* **2013**, *31*, 85; c) C. W. Lo, C. C. Wang, M. C. Lu, *Adv. Funct. Mater.* **2014**, *24*, 1211.

[10] P. Reimann, *Phys. Rep.* **2002**, *361*, 57.

[11] M. A. Stuart, W. T. Huck, J. Genzer, M. Muller, C. Ober, M. Stamm, G. B. Sukhorukov, I. Szleifer, V. V. Tsukruk, M. Urban, F. Winnik, S. Zauscher, I. Luzinov, S. Minko, *Nat. Mater.* **2010**, *9*, 101.

[12] a) H. Yang, H. Zhu, M. M. Hendrix, N. J. Lousberg, G. With, A. C. Esteves, J. H. Xin, *Adv. Mater.* **2013**, *25*, 1150; b) D. Roy, J. N. Cambre, B. S. Sumerlin, *Prog. Polym. Sci.* **2010**, *35*, 278; c) I. Tokarev, S. Minko, *Adv. Mater.* **2010**, *22*, 3446.

[13] R. R. Naik, M. O. Stone, *Mater. Today* **2005**, *8*, 18.

[14] A. Bagri, C. Mattevi, M. Acik, Y. J. Chabal, M. Chhowalla, V. B. Shenoy, *Nat. Chem.* **2010**, *2*, 581.

[15] R. Wang, K. Hashimoto, A. Fujishima, M. Chikuni, E. Kojima, A. Kitamura, M. Shimohigoshi, T. Watanabe, *Adv. Mater.* **1998**, *10*, 135.

[16] a) S. Daniel, M. K. Chaudhury, J. C. Chen, *Science* **2001**, *26*, 633; b) Y. Kong, Y. Liu, J. H. Xin, *J. Mater. Chem.* **2011**, *21*, 17978.

[17] R. Wang, K. Hashimoto, A. Fujishima, M. Chikuni, E. Kojima, A. Kitamura, M. Shimohigoshi, T. Watanabe, *Nature* **1997**, *388*, 431.

[18] K. Hashimoto, H. Irie, A. Fujishima, *Jpn. J. Appl. Phys.* **2005**, *44*, 8269.

[19] Y. Gao, Y. Masuda, K. Koumoto, *Langmuir* **2004**, *20*, 3188.

[20] M. Takeuchi, K. Sakamoto, G. Martra, S. Coluccia, M. Anpo, *J. Phys. Chem. B* **2005**, *109*, 15422.

[21] a) Y. T. Shen, D. Lei, W. Feng, *J. Mater. Chem. C* **2013**, *1*, 1926; b) J. S. Jeon, B. H. Kim, C. I. Park, S. Y. Seo, C. Kwak, S. H. Kim, S. W. Han, *Jpn. J. Appl. Phys.* **2010**, *49*, 031105; c) D. Lahiri, V. Subramanian, B. A. Bunker, P. V. Kamat, *J. Chem. Phys.* **2006**, *124*, 204720; d) M. G. Josifovska, V. Lazarov, J. Reynolds, V. V. Yakovlev, *Appl. Phys. Lett.* **2001**, *78*, 3298; e) L. H. Hanus, K. Sooklal, C. J. Murphy, H. J. Ploehn, *Langmuir* **2000**, *16*, 2621.

[22] H. G. Yang, C. H. Sun, S. Z. Qiao, J. Zou, G. Liu, S. C. Smith, H. M. Cheng, G. Q. Lu, *Nature* **2008**, *453*, 638.

[23] G. Liu, J. C. Yu, G. Q. Lu, H. M. Cheng, *Chem. Commun.* **2011**, *47*, 6763.

[24] a) S. Takahashi, H. Miura, H. Kasai, S. Okada, H. Oikawa, H. Nakanishi, *J. Am. Chem. Soc.* **2002**, *124*, 10944; b) F. Kim, J. H. Song, P. Yang, *J. Am. Chem. Soc.* **2002**, *124*, 14316; c) J. Zeng, C. Liu, J. Huang, X. Wang, S. Zhang, G. Li, J. Hou, *Nano Lett.* **2008**, *8*, 1318.

[25] D. Shakhvorostov, R. A. Nistor, L. K. Elbaum, G. J. Martyna, D. M. Newns, B. G. Elmegreen, X. Liu, Z. E. Hughes, S. Paul, C. Cabral, S. Raoux, D. B. Shrekenhamer, D. N. Basov, Y. Song, M. H. Muser, *Proc. Natl. Acad. Sci. USA* **2009**, *106*, 10907.
[26] J. Yu, W. Xiao, P. Zhou, M. Jaroniec, *J. Am. Chem. Soc.* **2014**, *136*, 8839.
[27] C. Liu, X. Han, S. Xie, Q. Kuang, X. Wang, M. Jin, Z. Xie, L. Zheng, *Chem. Asian J.* **2013**, *8*, 282.
[28] S. Leytner, J. T. Hupp, *Chem. Phys. Lett.* **2000**, *330*, 231.
[29] M. Lazzeri, A. Vittadini, A. Selloni, *Phys. Rev. B* **2001**, *63*, 155409.
[30] I. Sopyan, M. Watanabe, S. Murasawa, K. Hashimoto, A. Fujishima, *J. Photochem. Photobiol. A* **1996**, *98*, 79.
[31] G. L. Hornyak, J. Dutta, H. F. Tibbals, A. Rao, *Introduction to Nanoscience*, CRC Press, Boca Raton, FL **2011**.
[32] Y. Liang, H. Wang, H. S. Casalongue, Z. Chen, H. Dai, *Nano Res.* **2010**, *3*, 701.
[33] P. Day, A. Manze, Y. Zhang, *Microdroplet Technology: Principles and Emerging Applications in Biology and Chemistry*, Springer, New York, NY **2012**, Ch. 2.
[34] B. Bhushan, M. Nosonovsky, *Philos. Trans. R. Soc. A* **2010**, *368*, 4713.
[35] R. D. Noble, S. A. Stern, *Membrane Separation Technology: Principles and Applications*, Elsevier, Amsterdam, The Netherlands **1995**, Ch. 2.
[36] a) E. Honold, E. L. Skau, *Text. Res. J.* **1951**, *21*, 419; b) E. G. Burleigh, H. Wakeham, E. Honold, E. L. Skau, *Text. Res. J.* **1949**, *19*, 547.